Supporting Material for "Towards estimating the true duration of dendritic cell interactions with T cells"

by

Joost B. Beltman, Sarah E. Henrickson, Ulrich H. von Andrian,
Rob J. de Boer & Athanasius F.M. Marée

Supporting Figures

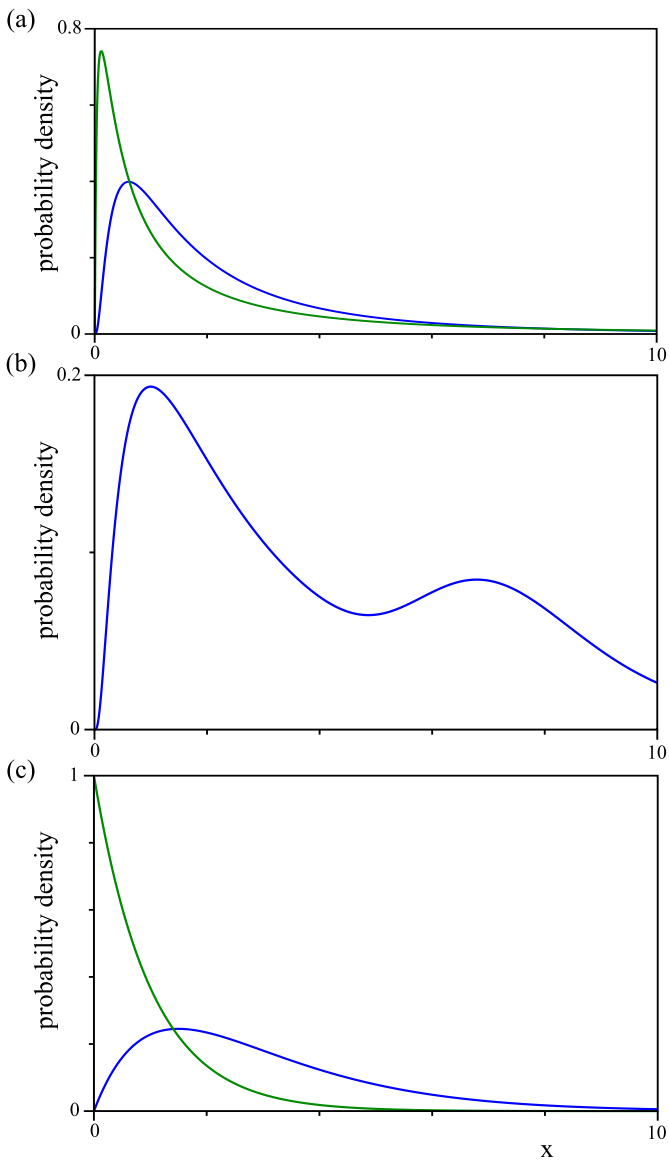

Figure S1. Typical distribution shapes. Shown is the typical shape of a lognormal distribution (a), the sum of two lognormal distributions (b), and a gamma distribution (c). Note that a gamma distribution can have two typical shapes (either it has a peak, or it declines monotonically). Distribution parameters: (a) blue line: $\mu = 0.5$, $\sigma = 1$; green line: $\mu = 0.1$, $\sigma = 1.5$. (b) $p = 0.8$, $\mu_1 = 1$, $\sigma_1 = 1$, $\mu_2 = 2$, $\sigma_2 = 0.2$. (c) blue line: $k = 2$, $\theta = 1.5$; green line: $k = 1$, $\theta = 1$. See section "Brief description of probability distributions" below for further explanation of these distributions.

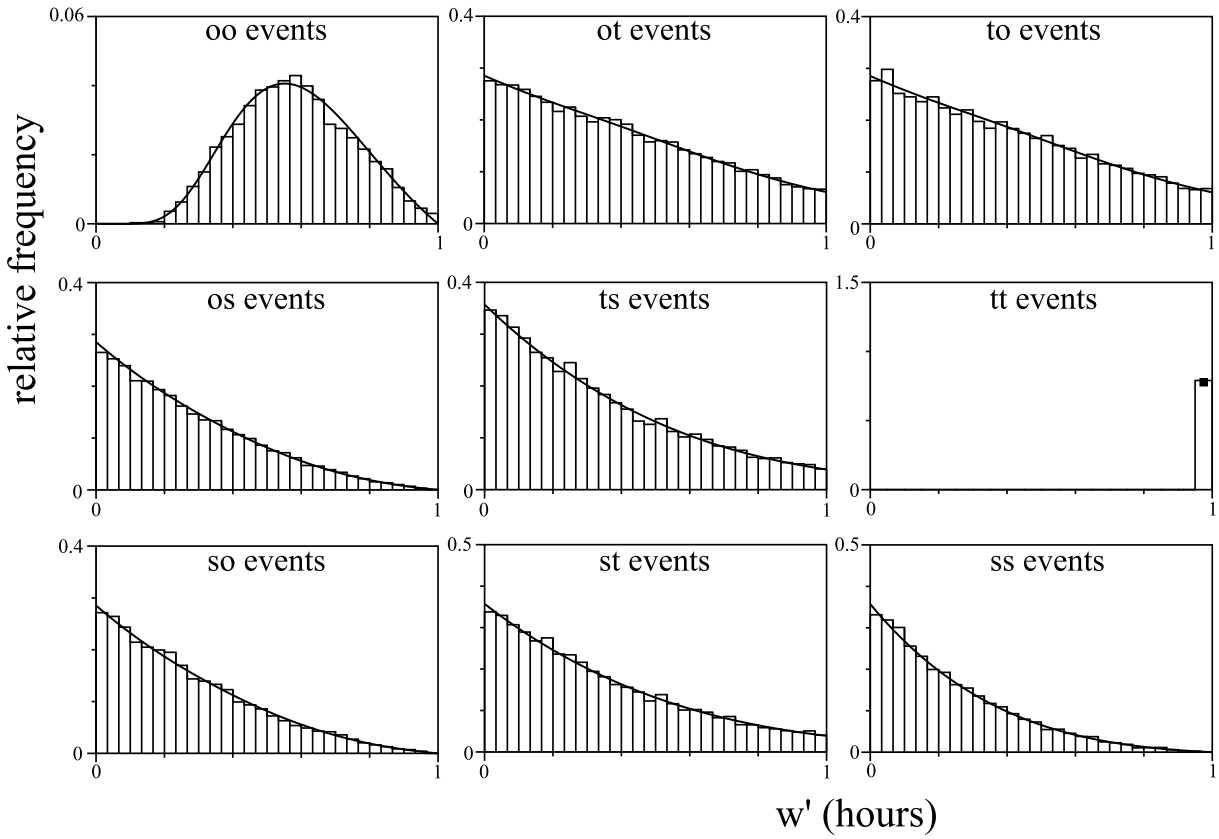

Figure S2. Testing the derived event distributions. Artificial contact data (consisting of $100,000$ data points) created using Monte Carlo simulations (explained in Supporting Text), plotted along with the expectation from the derived event distributions. This demonstrates the correctness of the derivation. To simulate these data and plot the predicted event distributions, we used a lognormal distribution with $\mu = 0.1$, $\sigma = 0.5$, and an entry and leaving rate of $\delta = 1.0$.

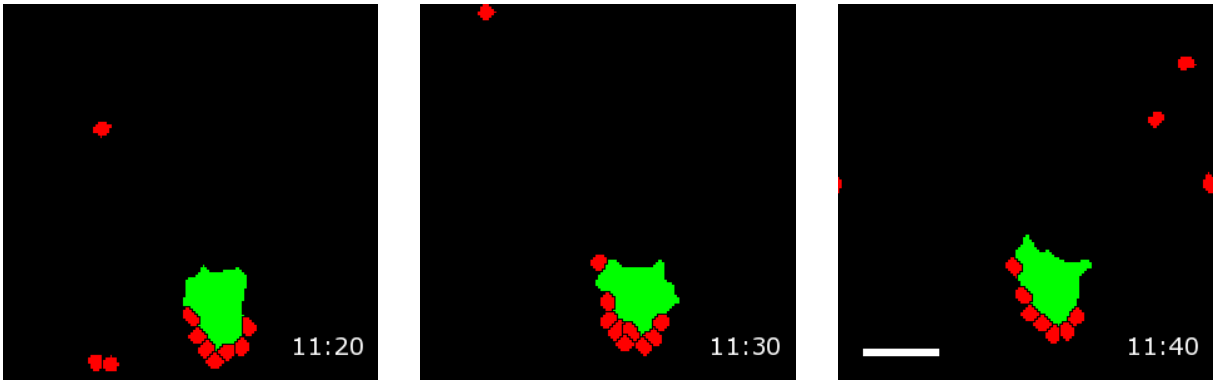

Figure S3. Cellular Potts Model simulations. Snapshots of 2D simulations at different time points showing *in silico* T cells (red) interacting with a single DC (green). Time is shown in hours:min. Scale bar: 30 μm. Parameter setting: $\gamma_{T,DC} = -300$ (see section "Cellular Potts Model simulations" below for other parameters).

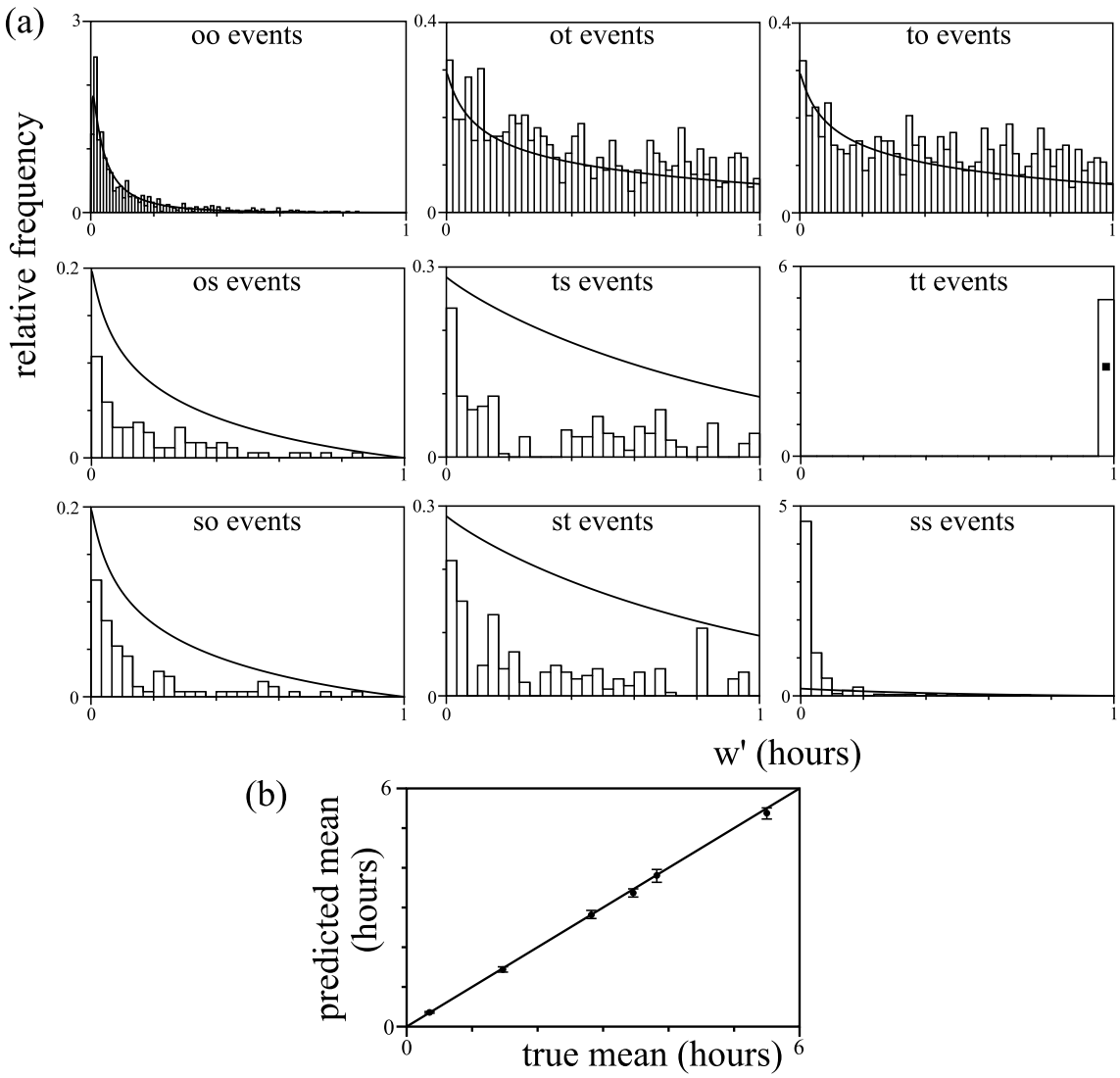

Figure S4. Poor fit when entry events are included in fitting procedure. The sum of two lognormal distributions was fitted to cellular interaction data from spatial simulations using our estimation method (1-hour observation window). We use all observed event distributions (i.e., including the entry event distributions) for the fitting procedure. (a) The observed distributions (types *oo*, *ot*, *to*, *tt*, *os*, *ts*, *so*, *st* and *ss*; see explanation in main text) are shown in histograms, along with the maximum likelihood fit (solid lines; filled square in middle rightmost panel). The observed contact time (w') is on the horizontal axes. Leaving out the entry events in the fitting procedure results in a much better fit (compare Fig. 4 in main text). (b) A comparison of the estimated average contact duration with the true average contact duration. The latter is calculated from the distribution of *oo* events in 100-hour simulations in which entry and exit is not taken into account. Note that, because the probability of observing these events declines with the duration of the event, to calculate the true average we assign different weights to each event (see main text). Error bars denote 95% CIs (determined with a bootstrap analysis).

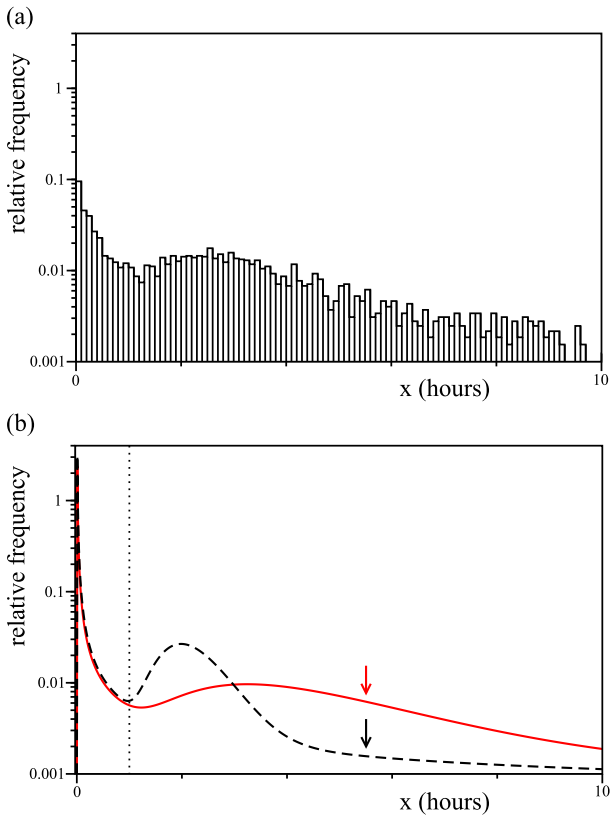

Figure S5. Accurate, robust estimate of average contact duration despite inaccurate fit of entire distribution. (a) A histogram of artificial data created with 100-hour CPM simulations with $\gamma_{T,DC} = -550$, which approaches the true distribution. The true contact time x is on the horizontal axis. (b) The 100-hour artificial data were split into 100 parts of one hour, and the true distribution was reconstructed from this. Shown are two fits of approximately equal likelihood (using the sum of two lognormal distributions as a basis). Despite the large difference with respect to the location and height of the second peak of the fits, in both cases the average is approximately 5.5 hours (average denoted by arrows). Dotted vertical line denotes the time window of imaging. Parameters: for the black dashed line $p \approx 0.50$, $\mu_1 \approx -0.39$, $\sigma_1 \approx 2.27$, $\mu_2 \approx 0.76$, $\sigma_2 \approx 0.26$, and for the red solid line $p \approx 0.45$, $\mu_1 \approx -0.66$, $\sigma_1 \approx 2.24$, $\mu_2 \approx 1.46$, $\sigma_2 \approx 0.49$. See section "Brief description of probability distributions" below for explanation of the parameters.

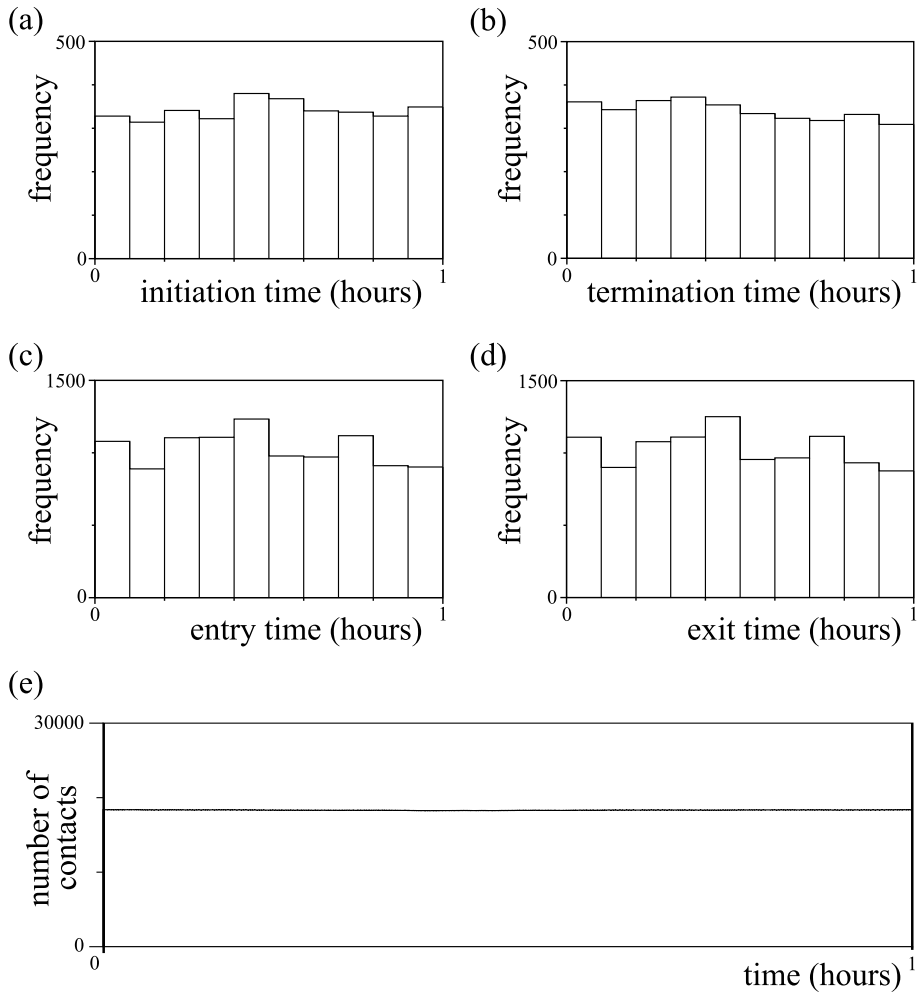

Figure S6. Checks performed on simulated contact data. (a–d) The frequency of observed initiation (a), termination (b), entry (c), and leaving (d) events over the time course of one hour of simulation time. (e) The number of observed conjugates present at each moment of simulation time. In all panels data from multiple simulations are combined. All shown distributions are approximately constant over time, as is to be expected. Parameter setting: $\gamma_{T,DC} = -550$.

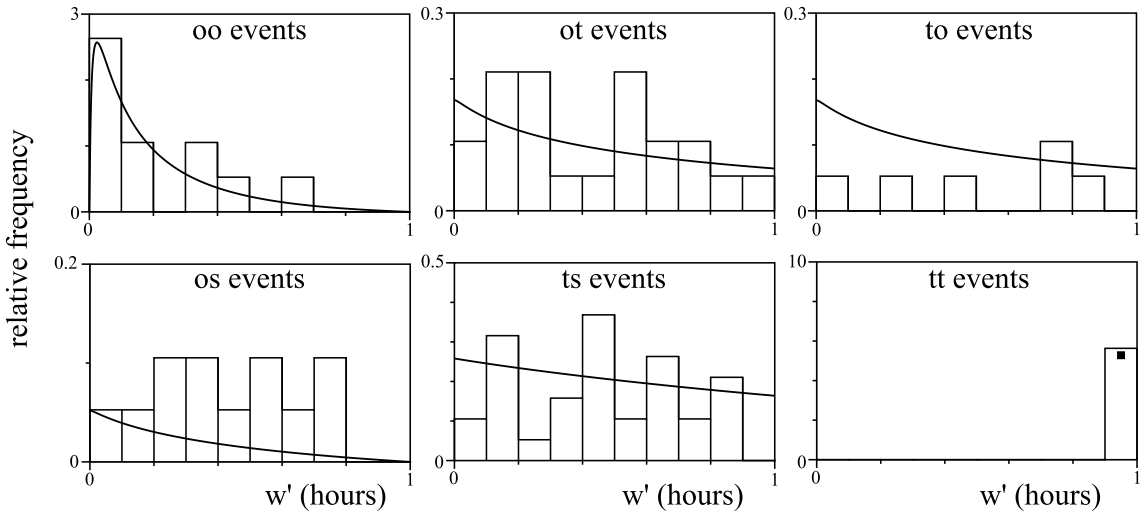

Figure S7. Analyzing an experimental subset with limited tissue drift. Our method to estimate the true contact time distribution, using the sum of two lognormal distributions as a basis, was applied to a subset of the "phase two" experiments of Henrickson et al. (2008) that exhibit limited tissue drift. The selection procedure for this subset was based on both a visual inspection of the videos (using a classification in five categories), and on the drift of DCs that appeared to be relatively stable. To quantify the drift of these DCs, three measures of the z-shift of the stable DCs were used: changes in their maximum intensity position as well as in the top and bottom positions within the imaged volume. We selected a subset of experiments for which each of the three measures (maximum intensity, top, and bottom) was at most 8 μm, and the visual classification was in the two categories of lowest tissue drift. To correct for mis-classifications at the end of the experiments (see main text), conjugates of which the termination was not observed in the last 200 seconds of each experiment were considered to be *ot*, *tt*, or *st* events. The experimentally observed distributions (types *oo*, *ot*, *to*, *tt*, *os* and *ts*; see explanation in main text) are shown in histograms, along with the maximum likelihood fit using the sum of two lognormal distributions (solid lines; filled square in lower rightmost panel). The observed contact time (w') is on the horizontal axis. The quality of the fit is clearly better compared to a fit of all phase two experiments (compare with Fig. 5b in main text; for each of the event distributions the lines pass better through the histograms, and the peaks in *os* and *ts* event distributions are not clearly present any more in Fig. S7). This suggests that tissue drift plays an important role in the discrepancies between model predictions and experimental data.

Supporting Video

Video S1. Movie of 100 hours showing *in silico* T cells (red) interacting with a single DC (green). T cell-DC contacts are of variable duration, which is due to stochastic membrane fluctuations. In the analysis the movie is split in 100 distinct 1-hour parts. Time is shown in hours:min. Scale bar: 30 μm. Parameter setting: $\gamma_{T,DC} = -300$.

Supporting Text

Expected number of observed events

Here we derive how many contacts one expects to observe in total during imaging experiments that are restricted in terms of both time and space (taking all possible event types that are discussed in the main text into account).

First consider the scenario that imaging allows us to only see contacts within a limited time window, for instance one hour (assuming that we are able to image an infinitely large space). One can now distinguish between two possibilities, namely conjugates for which the onset of interaction is observed or those that were already present at the start of imaging (the reasoning below is independent of whether the termination of events is observed or not). First consider those conjugates for which we have observed the onset of the interaction. Because the rate of initiation of new contacts is given by $Ng(x)$, this leads to $\int_{x=0}^{\infty} NTg(x)\,dx$ of such events (contacts initiated) during the entire experiment of T hours. Next consider the conjugates that were already present before we started imaging. How many of those conjugates will we observe in our imaging period? As an example, to observe a two-hour contact at the onset of imaging, it should have started somewhere between two and zero hours before imaging. Hence, the likelihood of observing an interaction at the start of imaging is proportional to the true length of the interaction x. In total, we expect to observe $\int_{x=0}^{\infty} Nxg(x)\,dx$ of such events. Adding up the two possibilities (events where the onset of interactions is either observed or not), this means that one expects to observe $\int_{x=0}^{\infty} NTg(x)\,dx + \int_{x=0}^{\infty} Nxg(x)\,dx = N\int_{x=0}^{\infty} (T+x)g(x)\,dx$ events in the imaged period. Normalizing this to the total number of true contacts initiated per hour (i.e., divide by N) we thus obtain $\int_{x=0}^{\infty} (T+x)g(x)\,dx$, which is equation (1d) in the main text.

When imaging is restricted in terms of both time and space, a third possibility for initial observation of events arises, namely that a conjugate moves into view during imaging. This does not affect the number of events already present at the onset of imaging or whose initiation is observed directly, so the total number of observed events per imaged volume increases in comparison with a situation where conjugates cannot move into view. To derive the frequency of conjugates that will be observed entering the field of view, it is instructive to consider what the relationship is between the (true) distribution of contact times and the frequency of conjugates that are expected to be present in a single imaging snapshot (i.e., at any point in time). As above, only contacts that started maximally x hours before the snapshot will be observed, so $\int_{x=0}^{\infty} Nxg(x)\,dx$ conjugates are expected to be observed at any point in time (including at the beginning). This relationship is independent of whether we have a limited field of view or not, because an equal number of conjugates will on average move into and out of view. Considering these movements to be constant over time and space, one can define a rate, δ, with which conjugates move into and out of view per hour. Given this rate, the number of conjugates leaving during the entire observation window is $\int_{x=0}^{\infty} \delta NTxg(x)\,dx$. Considering that our field of view is a small part of a homogeneous, larger region, this expression should also give the number of conjugates that enter the imaged volume. Adding this number to the other possible events gives the expected total number of observed events in case of imaging that is limited in time and space: $\int_{x=0}^{\infty} NTg(x)\,dx + \int_{x=0}^{\infty} Nxg(x)\,dx + \int_{x=0}^{\infty} \delta NTxg(x)\,dx = N\int_{x=0}^{\infty} (T + (1+\delta T)x)g(x)\,dx$. Normalizing this to the total number of true contacts initiated per hour we obtain $\int_{x=0}^{\infty} (T + (1+\delta T)x)g(x)\,dx$, which is equation (2g) in the main text.

Derivation of ss event distribution

Here we derive the expected distribution for *ss* events, given a true distribution $g(x)$. From the previous section ("Expected number of observed events") we know that $\delta TNxg(x)$ conjugates enter the imaged region during the time window of observation. Apart from their true contact time (x), two other factors are important in determining whether these conjugates will leave the field of view during imaging: (i) The time of entry. When a conjugate enters very early during the time window of observation, the probability that it moves out of view during imaging is high. If the conjugate enters late in the imaging experiment, it is likely that the experiment will be finished before the conjugate leaves (creating an *st* instead of an *ss* event). We therefore introduce the variable k to indicate the time of entry of the conjugate. Note that $0 \leq k \leq T$ because entry should occur before the end of imaging. (ii) The contact time that already elapsed at the moment of moving into view. If the conjugate enters while most of its contact time has already elapsed, it is likely that, instead of leaving the field of view, the termination of the conjugate will be observed (creating an *so* instead of an *ss* event). We therefore introduce the variable m to indicate the elapsed contact time at the moment of entering. The elapsed contact time must be between 0 and the true contact time, i.e., $0 \leq m \leq x$.

Because the dynamics are assumed to be homogeneous in both space and time, for conjugates that enter any elapsed contact time (m) as well as any time of entry (k) is equally likely. Thus, for each combination of elapsed contact time m and time of entry k, the number of conjugates that enter during the entire experiment is $\delta TNxg(x)$ divided by Tx, or simply $\delta Ng(x)$. The total number of conjugates entering during the experiment, normalized to the total number of true contacts initiated per hour can therefore be written as $\int_{x=0}^{\infty} \int_{m=0}^{x} \int_{k=0}^{T} \delta g(x)\, dk\, dm\, dx$, which equals $\int_{x=0}^{\infty} \delta Txg(x)\, dx$.

The observation of the termination of conjugates that enter allows for three possibilities (giving rise to *so*, *st*, or *ss* events). To derive the distribution of *ss* events, it helps to distinguish between two sub-classes of this event class. First, observations of which the termination would have been observed if the conjugate would not have left the imaged volume (below referred to as "missed" *so* events in the text, and ss_1 events in the equations). Second, observations that would otherwise have remained in view until the end of imaging (below referred to as "missed" *st* events in the text, and ss_2 events in the equations). We first derive how the length of observation (w') of "missed" *so* events depends on the true contact time (x), the elapsed contact time (m) and the time of entry (k). As explained step by step below, this relation becomes:

$$f_{ss_1}(w') = \int_{x=w'}^{T} \overbrace{\int_{m=0}^{x-w'}}^{\text{elapsed contact time}} \overbrace{\int_{k=0}^{T-x+m}}^{\text{time of entry}} \overbrace{\left(1-e^{-\delta(x-m)}\right)}^{\text{conjugate leaves}} \overbrace{\frac{\delta e^{-\delta w'}}{1-e^{-\delta(x-m)}}}^{\text{time of leaving}} \overbrace{\delta g(x)}^{\text{conjugate enters}} \, dk\, dm\, dx \tag{1a}$$

$$+ \int_{x=T}^{\infty} \int_{m=x-T}^{x-w'} \int_{k=0}^{T-x+m} \left(1-e^{-\delta(x-m)}\right) \frac{\delta e^{-\delta w'}}{1-e^{-\delta(x-m)}} \delta g(x)\, dk\, dm\, dx\,. \tag{1b}$$

The triple integrals result from the requirements for each of the three variables (x, m, and k) to contribute to an observed contact of length w'. First, the true contact time should be longer than the observed contact time, i.e., $x \geq w'$ (e.g., contacts of four minutes cannot be observed for five minutes). Therefore, we should only count contributions ranging from $\int_{x=w'}^{\infty} \ldots dx$. Contact times shorter than the time window of observation contribute

slightly differently than contact times longer than the imaging period, which is why we distinguish between the two parts, $\int\limits_{x=w'}^{T} \ldots dx$ and $\int\limits_{x=T}^{\infty} \ldots dx$ (equations (1a) and (1b)).

The reason for splitting up in two parts becomes clear in the requirements for the next variable, the elapsed contact time (m). This should be such that when a conjugate comes into view at least w' contact time is remaining. Therefore, we should only count the contributions coming from $\int\limits_{m=0}^{x-w'} \ldots dm$. For contact times longer than the imaging period, it should additionnally be the case that at most a contact time of T remains, because otherwise the event would be a "missed" *st* instead of a "missed" *so* event. This is taken into account by writing, for contact times longer than T, $\int\limits_{m=x-T}^{x-w'} \ldots dm$.

With respect to the third variable, the moment of entry (k), we know that the remaining time for the interaction equals $(x-m)$ (true minus elapsed contact time). In order to (potentially) observe the termination of a contact, its moment of entry should lie before $T-(x-m) = T-x+m$. Thus, we should only count the contributions coming from $\int\limits_{k=0}^{T-x+m} \ldots dk$.

The fourth term in the equation gives the probability that the conjugate leaves the imaged volume during the $(x-m)$ remaining contact time. This probability is $1-e^{-\delta(x-m)}$ (the fraction $e^{-\delta(x-m)}$ would be the probability that the termination of the contact will be observed, generating *so* events).

The fifth term defines the probability of a conjugate that both enters and leaves the field of view to leave after a specific time interval. The probability density of conjugate leaving at time w' is $\delta e^{-\delta w'}$. However, we need a correction factor because the total probability of conjugates that leave after any time (i.e., between time 0 and $(x-m)$) should sum up to unity. The probability density of leaving at time w' is therefore equal to $\left(\delta e^{-\delta w'}\right) / \left(1-e^{-\delta(x-m)}\right)$ (the integral $\int\limits_{w'=0}^{x-m} \left(\delta e^{-\delta w'}\right) / \left(1-e^{-\delta(x-m)}\right) dw'$ equals 1).

For the second sub-class of ss events the equation becomes:

$$
\begin{aligned}
f_{ss_2}(w') &= \int\limits_{x=w'}^{\overset{\text{true contact time}}{T}} \int\limits_{m=0}^{\overset{\text{elapsed contact time}}{x-w'}} \int\limits_{k=T-x+m}^{\overset{\text{time of entry}}{T-w'}} \left(1 - e^{-\delta(T-k)}\right) \frac{\delta e^{-\delta w'}}{1 - e^{-\delta(T-k)}} \, \overset{\text{conjugate leaves}}{\delta g(x)} \, dk \, dm \, dx \qquad \text{(2a)} \\
&+ \int\limits_{x=T}^{\infty} \int\limits_{m=x-T}^{x-w'} \int\limits_{k=T-x+m}^{T-w'} \left(1 - e^{-\delta(T-k)}\right) \frac{\delta e^{-\delta w'}}{1 - e^{-\delta(T-k)}} \, \delta g(x) \, dk \, dm \, dx \qquad \text{(2b)} \\
&+ \int\limits_{x=T}^{\infty} \int\limits_{m=0}^{x-T} \int\limits_{k=0}^{T-w'} \left(1 - e^{-\delta(T-k)}\right) \frac{\delta e^{-\delta w'}}{1 - e^{-\delta(T-k)}} \, \delta g(x) \, dk \, dm \, dx \, . \qquad \text{(2c)}
\end{aligned}
$$

This equation can be understood in a very comparable way as the equation for "missed" *so* events. The first question to pose is, which combinations of true contact time (x), elapsed contact time (m), and time of entry (k) would lead to the interaction still being observed at the end of imaging if the conjugate would not move out of view. As before, the true contact time should be longer than the observed interaction time, i.e., $x \geq w'$, and elapsed contact time should be such that when a conjugate comes into view at least w' contact time is remaining, i.e., $m \leq x - w'$. The time of entry (k) should be sufficiently early, such that at least w' time remains (otherwise an interaction of length w' could obviously not be observed). Furthermore, conjugates should come into view sufficiently late when the true contact time is shorter than the imaging period (i.e., when $x < T$), or when the true contact time is longer than the imaging period but less than T hours remains for the conjugate (i.e., when $x \geq T$ and $m > x - T$). Otherwise, "missed" *so*

events would be generated instead of "missed" *st* events, because the amount of contact time remaining would not allow observations until the end of the imaging experiment. In these cases (when $x < T$ or when $x \geq T$ and $m > x - T$) the integral for k becomes $\int\limits_{k=T-x+m}^{T-w'} \ldots dk$. The constraint on sufficiently late time of entry (k) is not present when, at the moment of movement into view, the remaining contact time is longer than T (which is the case when $x \geq T$ and $m \leq x-T$). Therefore, in that case the integral for k becomes $\int\limits_{k=0}^{T-w'} \ldots dk$.

The probability that a conjugate leaves depends on the time interval between entry and the end of the imaging period, because we are searching for "missed" *st* contacts. Thus, the fourth term in the equation becomes $\left(1 - e^{-\delta(T-k)}\right)$. Because the total probability of conjugates that leave after any time (that is, between time 0 and $T-k$ after entry) should sum up to unity, the probability density of leaving at time w' is $\left(\delta e^{-\delta w'}\right) / \left(1 - e^{-\delta(T-k)}\right)$ (the fifth term).

The remaining part of the derivation is straightforward integration. Combining the equations for "missed" *so* and "missed" *st* events we obtain:

$$f_{ss}(w') = \delta^2 e^{-\delta w'} \int\limits_{x=w'}^{T} \int\limits_{m=0}^{x-w'} \int\limits_{k=0}^{T-x+m} g(x)\, dk\, dm\, dx \tag{3a}$$

$$+ \delta^2 e^{-\delta w'} \int\limits_{x=T}^{\infty} \int\limits_{m=x-T}^{x-w'} \int\limits_{k=0}^{T-x+m} g(x)\, dk\, dm\, dx \tag{3b}$$

$$+ \delta^2 e^{-\delta w'} \int\limits_{x=w'}^{T} \int\limits_{m=0}^{x-w'} \int\limits_{k=T-x+m}^{T-w'} g(x)\, dk\, dm\, dx \tag{3c}$$

$$+ \delta^2 e^{-\delta w'} \int\limits_{x=T}^{\infty} \int\limits_{m=x-T}^{x-w'} \int\limits_{k=T-x+m}^{T-w'} g(x)\, dk\, dm\, dx \tag{3d}$$

$$+ \quad \delta^2 e^{-\delta w'} \int_{x=T}^{\infty} \int_{m=0}^{x-T} \int_{k=0}^{T-w'} g(x)\, dk\, dm\, dx\,. \tag{3e}$$

Integration along time of entry (k) then gives:

$$f_{ss}(w') = \delta^2 e^{-\delta w'} \int_{x=w'}^{T} \int_{m=0}^{x-w'} (T - x + m) g(x)\, dm\, dx \tag{4a}$$

$$+ \quad \delta^2 e^{-\delta w'} \int_{x=T}^{\infty} \int_{m=x-T}^{x-w'} (T - x + m) g(x)\, dm\, dx \tag{4b}$$

$$+ \quad \delta^2 e^{-\delta w'} \int_{x=w'}^{T} \int_{m=0}^{x-w'} (x - w' - m) g(x)\, dm\, dx \tag{4c}$$

$$+ \quad \delta^2 e^{-\delta w'} \int_{x=T}^{\infty} \int_{m=x-T}^{x-w'} (x - w' - m) g(x)\, dm\, dx \tag{4d}$$

$$+ \quad \delta^2 e^{-\delta w'} \int_{x=T}^{\infty} \int_{m=0}^{x-T} (T - w') g(x)\, dm\, dx\,. \tag{4e}$$

Combining equation (4a) with (4c), and equation (4b) with (4d), as well as integrating along elapsed contact time (m) one obtains:

$$f_{ss}(w') = \delta^2 e^{-\delta w'} \int_{x=w'}^{T} (T - w')(x - w') g(x)\, dx \tag{5a}$$

$$+ \quad \delta^2 e^{-\delta w'} \int_{x=T}^{\infty} \left((T - w')(x - w') - (T - w')(x - T) \right) g(x)\, dx \tag{5b}$$

$$+ \quad \delta^2 e^{-\delta w'} \int_{x=T}^{\infty} (T - w')(x - T) g(x)\, dx\,, \tag{5c}$$

which sums up to

$$f_{ss}(w') = \delta^2 e^{-\delta w'}(T - w') \int_{x=w'}^{\infty} (x - w') g(x)\, dx\,. \tag{6}$$

Despite the complicated derivation, one ends up with a simple equation for $f_{ss}(w')$, resembling a combination of equations (2c) and (2d) in the main text. As expected, adding up the $\int_{w'=0}^{T} \ldots dw'$ integrals for all event classes gives the total number of events derived in the previous section (see also equation (2g) in main text).

Reconstruction of the true distribution

Here we discuss a partly non-parametric way to reconstruct the true distribution from the observed event distributions alternative from the (parametric) maximum likelihood estimation discussed in the main text. Consider first the case of imaging limited in time. In the reconstruction it is important to distinguish between contacts lasting shorter than the imaging period (referred to as "head" of the true distribution) and longer than the imaging period (referred to as "tail" of the true distribution). Starting with the observed distribution of *oo* events, one can see from equation (1a) in the main text that the head of the true distribution (where $x < T$) equals $f_{oo}(w)/(T - w)$. This is a correction that should always be done but has so far not been performed on experimental data (see Mempel et al., 2004; Miller et al., 2004a,b; Hugues et al., 2004; Mempel et al., 2006; Mrass et al., 2006; Tadokoro et al., 2006; Garcia et al., 2007; Celli et al., 2007; Allen et al., 2007; Schwickert et al., 2007; Hugues et al., 2007; Guarda et al., 2007; Henrickson et al., 2008; Scholer et al., 2008). How can the observed f_{ot}, f_{to}, and f_{tt} distributions subsequently be used to reconstruct the tail (i.e., $x > T$) of the true distribution? From the derivation of equation (1b) in the main text we know that $f_{ot}(w)$ and $f_{to}(w)$ consists

of two parts, contributed by interactions that are either shorter or longer than the time window of imaging. We can next use the f_{oo}-based prediction for the head of the true distribution to calculate which part of $f_{ot}(w)$ and $f_{to}(w)$ it explains (because one can now calculate $\int_{x=w}^{T} g(x)\,dx$). The difference between the observed distributions for $f_{ot}(w)$ and $f_{to}(w)$ and the contribution by the head then gives the contribution by the tail of the true distribution (remember that the latter should be flat). Because the frequency of to (or ot) events contributed by the tail is $\int_{x=T}^{\infty} g(x)\,dx$, this also gives the expected frequency of contacts in the tail. How can we make a prediction for the shape of the tail of the true distribution? We now have two values, namely $\int_{x=T}^{\infty} g(x)\,dx$ (the frequency of observed to and ot events) and $\int_{x=T}^{\infty} (x-T)g(x)\,dx$ (the frequency of observed tt events), which does not allow to determine the value for each contact duration x. However, given a certain type of distribution, a best fit can be found.

The advantage of this "reconstruction" method is that no assumptions are required for the shape of the head of the true distribution (i.e., it is non-parametric). However, the reconstruction becomes complicated when conjugates are able to leave or enter the imaged volume. In that case, from equation (2a) in the main text one can see that the head of the true distribution equals $f_{oo}(w)/((T-w)e^{-\delta w'})$. In order to calculate that, we need to have an estimate for the rate δ with wich conjugates enter or leave the imaged region. There are multiple ways to make such an estimate. One way is to divide the number of events that leave the imaged volume during the observation window (os, ts, or ss events) by the total number of conjugates present at any moment in time (for the latter the average of all time points can be calculated). Because ss events will introduce an error in this estimate (due to their initial position that is close to one of the borders), it is better to leave them out of the calculation for estimating δ completely. This can be done by dividing the total number of os and ts events (i.e., leave out the ss events) by the total number of conjugates

present at any point in time that are not ss events. Having thus obtained an estimate for δ, the head of the true distribution can be estimated. Using this, we can calculate the part that the head contributes to the event distributions of classes ot, to, os, so, ts, st and ss. As before, the other part of these distributions is a consequence of the tail of the true distribution. Therefore, the number $\int_{x=T}^{\infty} g(x)\,dx$ can be calculated, but it is unclear whether one should use for this the number resulting from the ot, the to, the os, or the so event distributions (equations (2b) and (2c) in main text), or some kind of weighted average of these numbers. In combination with the estimate for $\int_{x=T}^{\infty} (x-T)g(x)\,dx$ that comes from the tt event distribution (equation (2f) in main text), we can find a best fit. In this procedure we have not used the estimate for $\int_{x=T}^{\infty} (x-w')g(x)\,dx$ that we could have obtained from either of the ts, st, or ss event distributions (equations (2d) or (2e) in main text). In summary, it is possible to perform a "reconstruction" of the true distribution, but this involves many steps where errors in estimates will accumulate on top of the errors of previous steps. Furthermore, classes of events contribute as a whole rather than as individual observations to the final estimate. Finally, combining experiments with different imaging durations is problematic, because one should then take into account that within each event class there exist sub-classes for which observations differ in the time window T. For these reasons, it is in our opinion better to take the maximum likelihood approach that we use in the main text. Even though that procedure requires as input a certain shape for the entire true distribution (i.e., it is parametric), it is more straightforward, each observation contributes individually (i.e., in a statistically fair way) to the estimate for the true distribution, and one can readily combine contact data coming from experiments of different duration.

Generating artificial contact data

We take two appraoches to test the validity of our method to estimate the true contact time distribution. First, we use Monte Carlo simulations according to the situation we consider to test the correctness of the derivation of the equations. Second, we use spatial simulations of motile T cells and DCs to generate more realistic contact data. These approaches are described below in detail.

Monte Carlo simulations

To generate cellular contact data we consider a time axis where imaging occurs from time point 0 to time point T. We further consider two volumes, one representing the imaged volume, and the other representing the rest of the volume that we do not image. The simplest way to create an approximately equal number of border crossings in both directions from the viewpoint of individual conjugates is to consider two volumes of equal size.

We sample contact durations of conjugates from a known distribution (e.g., a lognormal distribution), which is thus equal to the true distribution for the particular parameter setting that is being simulated. For each duration we also sample a time point at which that interaction begins. For this we use a uniform distribution with maximum T (because any contact starting after that would not be observed) and an appropriate, negative value for the minimum: For the value of this minimum we take the contact duration for which 99.9% of the distribution falls below it. As such, the minimum will be sufficiently low such that we are not introducing a bias with respect to the starting point of long-lasting interactions. Further, the minimum is not too low as we would then generate many data points that we cannot use because the termination of the interaction is before we

start imaging (time point 0). Each contact duration begins with probability 0.5 inside, or otherwise outside, the imaged volume. Conjugates keep switching between the two volumes until they have terminated. The time at which the next switch occurs is sampled from an exponential distribution with rate of switching δ. We monitor all interactions that occur inside the imaged volume as well as during the observation period. Hence, all interactions that have already ended before time point 0, or that occur entirely outside of the imaged volume, do not end up in one of the nine possible event classes. Note that a single conjugate is able to generate multiple data points because it can switch multiple times between the volumes.

Generating the data in this manner is conform the situation for which we derived the equations for the nine event classes. Plotting the generated contact data along with the predicted event distributions using the input distribution parameters shows a near-perfect accordance (Fig. S2), which demonstrates the correctness of our derivations.

We next investigate whether fitting of such an idealized data set gives approximately the same result when we leave out the entry event distributions from the fitting procedure or not. In other words, we test whether we can leave out the entry events without introducing a bias. Applying our maximum likelihood approach to estimate the true distribution indeed leads to a similar result with or without entry events (see Fig. S2). For instance, using a lognormal distribution with $\mu = 0.1$ and $\sigma = 0.5$, and a switching rate of $\delta = 1$ as in Figure S2, we obtain $\mu \approx 0.11$, $\sigma \approx 0.50$ and $\delta \approx 1.00$ as the best fit whether entry events are included or not. This confirms that entry events can be left out without introducing a bias. Based on verbal reasoning and on the results of our more realistic spatial simulations we argue that the best strategy for experimental data sets is to leave out the entry events from the fitting procedure (see main text and compare Fig. S4 with Fig. 4).

Cellular Potts Model simulations

To further test the validity of the method to estimate the true distribution of contact times, we used simulations based on our previously published lymph node simulations using the Cellular Potts Model (CPM) (Beltman et al., 2007b,a). The CPM (Graner and Glazier, 1992; Glazier and Graner, 1993) considers a lattice where multiple connected sites (with 2D coordinates i, j) together comprise a cell of type $\tau(\sigma)$, where σ represents the cell identification number. Sites that contact other cells or extracellular matrix have a surface energy with their direct surroundings. Cells are considered to try to minimize their surface energies over time. To determine how an extension of a lattice site into a random neigbour, which is constantly attempted during a simulation, would change the surface energy, one calculates the so-called Hamiltonian:

$$H = \sum_{ij} \sum_{i'j'} J_{\tau(\sigma_{ij}),\tau(\sigma_{i'j'})}(1 - \delta_{\sigma_{ij},\sigma_{i'j'}}) + \sum_{\sigma} \lambda(a_\sigma - A_\sigma)^2 \quad , \tag{7}$$

where the first term represents the sum of all surface energies J, and the second term is required to keep cells of actual area a close to their target area A. Further, δ_K is the Kronecker delta, and $\sigma_{i'j'}$ sums over all 8 neighbours in the 3×3 neighbourhood. The probability that a lattice site is copied to a neighbouring site is one if $\Delta H < 0$, and $e^{-(\Delta H)/T_B}$ otherwise, where ΔH is the change in H due to the considered modification, and T_B represents the membrane fluctuation amplitude of cells.

As in Beltman et al. (2007b,a) we extend the CPM to simulate T cell motility and the behaviour of DC dendrites. T cells are considered to exhibit a polarity, which makes extensions of lattice sites that are approximately in the direction of the polarity more likely than other extensions. This is implemented by the following extra term in ΔH for

T cells:

$$\Delta H \quad = \quad -\mu \; cos(\alpha) \quad , \tag{8}$$

where μ is the "directional propensity" of cells, and α is the angle between polarity and the considered displacement vector (the vector given by the coordinate of the position whose modification is considered and the mean position of the cell). The polarity of T cells is intially random, but is updated each Δt seconds to become the displacement vector of the previous period. To describe cell turning in a realistic way, the actual μ value of a T cell is also adjusted according to its recent displacement: $\mu = \mu_{max} \; e^{-\rho(1-cos \; \beta)}$, where μ_{max} is the maximum directional propensity T cells can obtain, β is the angle between the displacement and target vector of the previous period, and ρ determines how rapidly the directional propensity declines when a turn is occurring. A T cell that receives a stop signal because it is in contact with a DC, turns its directional propensity to 0, i.e., looses its directional motility. When the contact subsequently breaks, the directional propensity is "turned on", at a value according to its recent, usually small, displacement (see above formula).

We describe dendrites of *in silico* DCs by explicitly defining multiple ($N_{bundles}$) thin actin bundles that start growing at a position "inside" the cell, and in a random, straight direction. Each time step actin bundles extend themselves a single position into their direction of movement, provided that the site they are growing into belongs to the DC. When this is not the case, the dendrite will try again the following time step. When extension of an actin bundle fails for 20 time steps in a row, it will start retracting. Otherwise, the bundle retracts after a maximum growth period of 100 time steps (this determines the maximum length a dendrite can obtain, although it will generally be

much shorter). Actin bundles pull themselves back in reverse order as they have grown. Retraction takes place with a single position per time step, with probability p_{retr} (this parameter determines the speed of retraction). As soon as an actin bundle has pulled itself back completely, a new bundle starts to extend. New dendrites start out from the current mean DC position. The pushing of actin bundles against the DC cell membrane is modelled by increasing the likelihood that membrane elements grow into positions adjacent to a bundle. This is done by incorporating an extra term in ΔH: when an extension of membrane into a bundle-neighbouring site is considered, ΔH is decreased with E_{extend} (this parameter determines how much DCs are inclined to extend dendrites). Furthermore, to prevent the breaking of dendrites, membrane elements adjacent to actin bundles are required to remain intact.

Distinct from our previous 3D LN simulations (Beltman et al., 2007b,a), in the current paper we combine data from multiple 2D simulations in which only a limited number of cells are described (Supporting Fig. S3). This was done to enable fast generation of a large number of data points. We define exiting and entering of conjugates to occur when the centre of mass of a DC crosses one of the borders of the space (the conjugates with the T cells that are attached to it at that moment enter or leave). Because DC movement (due to stochastic membrane fluctuations) is required to obtain such conjugate entry and exit, we do not fix the position of DCs around a certain position (as was done in Beltman et al. (2007a)) but let them move freely. This is achieved by considering new dendrites to grow out from the current centre of mass of the DC. However, that entails that interactions between T cells and DCs remain relatively brief (due to competition with other DCs and T cells (Beltman et al., 2007a)). Because a rigorous test of the method requires long-lasting interactions, in each simulation we used a single DC along with 10 T cells in a $150\mu\text{m}\times150\mu\text{m}$ space (one lattice site equals $1\mu\text{m}^2$) that further contains only extracellular matrix rather than other cells (thus enabling long interactions). Cells are initialized at a

random position as a 9 μm^2 block, and subsequently grow to their target areas (40 μm^2 for T cells and 600 μm^2 for DCs). To obtain multiple, different distributions of contact lengths, we vary the surface adhesion between T cells and DCs ($\gamma_{T,DC}$) from -100 to -550. The surface energies between T cells themselves and between DCs themselves are kept at 1000. Other parameters: $N_{bundles} = 30$, $E_{extend} = 1000$, $p_{retr} = 0.3$, $\mu_{max} = 800$, $\Delta t = 20s$, $T = 100$, $\rho = 3$, $\lambda = 100$.

Brief description of probability distributions

Here, we briefly describe the distributions that we use in the main text to fit the contact data (lognormal distribution, sum of two lognormal distributions, and gamma distribution). These are all continuous distributions of variable x.

The lognormal distribution is described by the probability density function:

$$f(x) = \frac{e^{-(-\mu+\ln x)^2/(2\sigma^2)}}{\sqrt{2\pi}x\sigma}\,, \tag{9}$$

where μ ($-\infty < \mu < \infty$) and σ ($\sigma > 0$) are the mean and standard deviation of the variable's logarithm. The shape of the lognormal distribution is more or less skewed with a single peak at relatively low x values (the location of the peak varies with the parameters, see Supporting Fig. S1a).

The sum of two lognormal distributions can be described by the probability density function:

$$f(x) = p\,\frac{e^{-(-\mu_1+\ln x)^2/(2\sigma_1^2)}}{\sqrt{2\pi}x\sigma_1} + (1-p)\,\frac{e^{-(-\mu_2+\ln x)^2/(2\sigma_2^2)}}{\sqrt{2\pi}x\sigma_2}\,, \tag{10}$$

where μ_1, μ_2 ($-\infty < \mu_1, \mu_2 < \infty$), σ_1 and σ_2 ($\sigma_1, \sigma_2 > 0$) are defined analogously to the parameters of the lognormal distribution. The parameter p ($0 \leq p \leq 1$) determines the relative impact of the two separate lognormal parts. This construction allows one to describe a distribution with two peaks (Supporting Fig. S1b). For our case of contact duration these can be interpreted as brief and long contacts, respectively.

The gamma distribution is described by the probability density function:

$$f(x) = x^{k-1} \frac{e^{-x/\theta}}{\theta^k \Gamma(k)}, \tag{11}$$

with scale parameter θ ($\theta > 0$) and scale parameter k ($k > 0$), and where $\Gamma(z)$ is the gamma function ($\Gamma(z) = \int_0^\infty t^{z-1} e^{-t}\, dt$). The parameter k determines the shape of the distribution, which can take two basic forms (see Supporting Fig. S1c). For $k > 1$, the distribution has a peak, whereas for $k \leq 1$, the distribution declines monotonically with a finite value at $x = 0$ (for $k = 1$ one obtains an exponential distribution).

Example calculation for one contact data point

Suppose that we performed an imaging experiment lasting 75 minutes (1.25 hours). One of the observations we made was a *to* event that we saw ending at time point 35 minutes (i.e., a duration of 0.58 hours). How can we calculate the probability density for this precise observation?

Choosing a lognormal distribution as a basis for our estimation procedure, we first calculate $f_{to}(w')$ for that case. We obtain:

$$
\begin{aligned}
f_{ot}(w') &= e^{-\delta w'} \int_{x=w'}^{\infty} g(x)\,dx && \text{(12a)}\\
&= e^{-\delta w'} \int_{x=w'}^{\infty} \frac{e^{-(-\mu+\ln x)^2/(2\sigma^2)}}{\sqrt{2\pi}x\sigma}\,dx && \text{(12b)}\\
&= \frac{1}{2}\,e^{-\delta w'}\left(1+\operatorname{erf}\left(\frac{\mu-\ln(w')}{\sqrt{2}\sigma}\right)\right), && \text{(12c)}
\end{aligned}
$$

where $\operatorname{erf}(z)$ is the error function ($\operatorname{erf}(z) = 2/\sqrt{\pi} \int_{t=0}^{z} e^{-t^2}\,dt$). The total number of events one expects to observe during imaging normalized to the total number of true contacts initiated per hour (taking into account all events minus those for which conjugates enter, becomes):

$$
\begin{aligned}
\int_{x=0}^{\infty} (T+x)g(x)\,dx &= \int_{x=0}^{\infty} (T+x)\frac{e^{-(-\mu+\ln x)^2/(2\sigma^2)}}{\sqrt{2\pi}x\sigma}\,dx && \text{(13a)}\\
&= T + e^{\mu+\sigma^2/2}\,. && \text{(13b)}
\end{aligned}
$$

We divide the distribution of *to* events (equation (12c)) by the normalized total number of expected events (equation (13b)). Thus, the *to* event distribution (corrected to obtain probability densities) becomes:

$$
\frac{e^{-\delta w'}\left(1+\operatorname{erf}\left(\frac{\mu-\ln(w')}{\sqrt{2}\sigma}\right)\right)}{2(T+e^{\mu+\sigma^2/2})}\,. \qquad (14)
$$

Substituting $T = 1.25$ hours and $w = 0.58$ hours, one can calculate the probability density of the observed *to* event for particular values of μ, σ and δ, (for instance, when $\mu = 0.5$,

$\sigma = 2$ and $\delta = 0.1$ we would obtain 0.049). Performing the same procedure for all the other observed events, and subsequently summing the logarithms of all the obtained values gives the loglikelihood for these particular values of μ, σ and δ. Finally, the distribution parameters for which the loglikelihood is at its maximum is obtained with the assistance of an optimization algorithm (in our case this was done using the `bbmle` package in R).

Observed contact time distributions

Here we give the analytical solutions for the observed contact time distributions (equations (2a) to (2f) in main text) for the cases of a lognormal distribution and a gamma distribution. For the sum of two lognormal distributions this can also be solved analytically using a calculus software package (available on request).

Lognormal distribution

Substituting a lognormal distribution with parameters μ and σ (see section describing probability distributions) into equations (2a) to (2f) from the main text gives:

$$f_{oo}(w') = \frac{e^{-\frac{(-\mu+\ln[w'])^2}{2\sigma^2}-\delta w'}(T-w')}{\sqrt{2\pi}\sigma w'} \tag{15a}$$

$$f_{ot}(w') = f_{to}(w') = \frac{1}{2}e^{-\delta w'}\left(1+\operatorname{erf}\left[\frac{\mu-\ln[w']}{\sqrt{2}\sigma}\right]\right) \tag{15b}$$

$$f_{os}(w') = f_{so}(w') = \frac{1}{2}e^{-\delta w'}\delta\,(T-w')\left(1+\operatorname{erf}\left[\frac{\mu-\ln[w']}{\sqrt{2}\sigma}\right]\right) \tag{15c}$$

$$\begin{aligned} f_{ts}(w') = f_{st}(w') &= \frac{1}{2}e^{-\delta w'}\delta\,\cdot \\ &\left(e^{\mu+\frac{\sigma^2}{2}}\left(1+\operatorname{erf}\left[\frac{\mu+\sigma^2-\ln[w']}{\sqrt{2}\sigma}\right]\right)-\right. \\ &\left.\left(1+\operatorname{erf}\left[\frac{\mu-\ln[w']}{\sqrt{2}\sigma}\right]\right)w'\right) \end{aligned} \tag{15d}$$

$$
\begin{aligned}
f_{ss}(w') &= \frac{1}{2}e^{-\delta w'}(T-w')\delta^2 \cdot \\
&\left(-w'\left(1+\mathrm{erf}\left[\frac{\mu-\ln[w']}{\sqrt{2}\sigma}\right]\right)+\right. \\
&\left.e^{\mu+\frac{\sigma^2}{2}}\left(1+\mathrm{erf}\left[\frac{\mu+\sigma^2-\ln[w']}{\sqrt{2}\sigma}\right]\right)\right)
\end{aligned}
\tag{15e}
$$

$$
f_{tt}(w') = \begin{cases} 0 & \text{if } w' < T \\ \frac{1}{2}e^{-\delta T}\cdot & \\ \left(-T\left(1+\mathrm{erf}\left[\frac{\mu-\ln[T]}{\sqrt{2}\sigma}\right]\right)+\right. & \\ \left.e^{\mu+\frac{\sigma^2}{2}}\left(1+\mathrm{erf}\left[\frac{\mu+\sigma^2-\ln[T]}{\sqrt{2}\sigma}\right]\right)\right) & \text{if } w' = T, \end{cases}
\tag{15f}
$$

where $\mathrm{erf}(z)$ is the error function ($\mathrm{erf}(z) = 2/\sqrt{\pi}\int_{t=0}^{z} e^{-t^2}\,dt$).

The total number of events one expects to observe during imaging normalized to the total number of contacts initiated per hour, i.e., the sum of the integrals $\int_{w'=0}^{T} f_{oo}(w')\,dw' + \cdots + \int_{w'=0}^{T} f_{tt}(w')\,dw'$, equals $T + e^{\mu+\frac{\sigma^2}{2}}(1+T\delta)$. Calculating the total while leaving out the entry events gives $T + e^{\mu+\frac{\sigma^2}{2}}$.

Gamma distribution

Substituting a gamma distribution with parameters μ and σ (see section describing probability distributions) into equations (2a) to (2f) from the main text gives:

$$
f_{oo}(w') = \frac{e^{-\frac{w'}{\beta}-\delta w'}(T-w')w'^{-1+\alpha}\beta^{-\alpha}}{\Gamma[\alpha]}
\tag{16a}
$$

$$
f_{ot}(w') = f_{to}(w') = \frac{e^{-\delta w'}\Gamma\left[\alpha, \frac{w'}{\beta}\right]}{\Gamma[\alpha]}
\tag{16b}
$$

$$
f_{os}(w') = f_{so}(w') = \frac{e^{-\delta w'}(T-w')\delta\Gamma\left[\alpha, \frac{w'}{\beta}\right]}{\Gamma[\alpha]}
\tag{16c}
$$

$$f_{ts}(w') = f_{st}(w') = \frac{e^{-\delta w'}\delta\left(-w'\Gamma\left[\alpha, \frac{w'}{\beta}\right] + \beta\Gamma\left[1+\alpha, \frac{w'}{\beta}\right]\right)}{\Gamma[\alpha]} \tag{16d}$$

$$f_{ss}(w') = \frac{e^{-\delta w'}(T-w')\delta^2\left(-w'\Gamma\left[\alpha, \frac{w'}{\beta}\right] + \beta\Gamma\left[1+\alpha, \frac{w'}{\beta}\right]\right)}{\Gamma[\alpha]} \tag{16e}$$

$$f_{tt}(w') = \begin{cases} 0 & \text{if } w' < T \\ \frac{e^{-\delta T}\left(-T\Gamma\left[\alpha, \frac{T}{\beta}\right] + \beta\Gamma\left[1+\alpha, \frac{T}{\beta}\right]\right)}{\Gamma[\alpha]} & \text{if } w' = T, \end{cases} \tag{16f}$$

where $\Gamma(y)$ is the gamma function ($\Gamma(y) = \int_{t=0}^{\infty} t^{y-1}e^{-t}\,dt$), and $\Gamma(y,z)$ is the upper incomplete gamma function ($\Gamma(y,z) = \int_{t=z}^{\infty} t^{y-1}e^{-t}\,dt$).

The total number of events one expects to observe during imaging normalized to the total number of contacts initiated per hour, i.e., the sum of the integrals $\int_{w'=0}^{T} f_{oo}(w')\,dw' + \cdots + \int_{w'=0}^{T} f_{tt}(w')\,dw'$, equals $T + \alpha\beta(1+\delta T)$. Calculating the total while leaving out the entry events gives $T + \alpha\beta$.

Supporting references

Allen, C. D., Okada, T., Tang, H. L., Cyster, J. G., 2007. Imaging of germinal center selection events during affinity maturation. Science 315 (5811), 528–31.

Beltman, J. B., Marée, A. F. M., De Boer, R. J., 2007a. Spatial modelling of brief and long interactions between T cells and dendritic cells. Imm. Cell Biol. 85 (4), 306–314.

Beltman, J. B., Marée, A. F. M., Lynch, J. N., Miller, M. J., De Boer, R. J., 2007b. Lymph node topology dictates T cell migration behaviour. J. Exp. Med. 204 (4), 771–780.

Celli, S., Lemaitre, F., Bousso, P., 2007. Real-time manipulation of T cell-dendritic cell interactions in vivo reveals the importance of prolonged contacts for $CD4^+$ T cell activation. Immunity 27 (4), 625–34.

Garcia, Z., Pradelli, E., Celli, S., Beuneu, H., Simon, A., Bousso, P., 2007. Competition for antigen determines the stability of T cell-dendritic cell interactions during clonal expansion. Proc. Natl. Acad. Sci. USA 104 (11), 4553–8.

Glazier, J. A., Graner, F., 1993. Simulation of the differential adhesion driven rearrangement of biological cells. Phys. Rev. E 47 (3), 2128–2154.

Graner, F., Glazier, J. A., 1992. Simulation of biological cell sorting using a two-dimensional extended potts model. Phys. Rev. Lett. 69, 2013–2016.

Guarda, G., Hons, M., Soriano, S. F., Huang, A. Y., Polley, R., Martin-Fontecha, A., Stein, J. V., Germain, R. N., Lanzavecchia, A., Sallusto, F., 2007. L-selectin-negative $CCR7^-$ effector and memory $CD8^+$ T cells enter reactive lymph nodes and kill dendritic cells. Nat. Immunol. 8 (7), 743–52.

Henrickson, S., Mempel, T., Mazo, I., Liu, B., Artyomov, M., Zheng, H., Peixoto, A., Flynn, M., Senman, B., Junt, T., Wong, H., Chakraborty, A., von Andrian, U., 2008. T cell sensing of antigen dose governs interactive behavior with dendritic cells and sets a threshold for T cell activation. Nat. Immunol. 9 (3), 282–91.

Hugues, S., Fetler, L., Bonifaz, L., Helft, J., Amblard, F., Amigorena, S., 2004. Distinct T cell dynamics in lymph nodes during the induction of tolerance and immunity. Nat. Immunol. 5 (12), 1235–1242.

Hugues, S., Scholer, A., Boissonnas, A., Nussbaum, A., Combadiere, C., Amigorena, S., Fetler, L., 2007. Dynamic imaging of chemokine-dependent $CD8^+$ T cell help for $CD8^+$ T cell responses. Nat. Immunol. 8 (9), 921–30.

Mempel, T. R., Henrickson, S. E., von Andrian, U. H., 2004. T cell priming by dendritic cells in lymph nodes occurs in three distict phases. Nature 427, 154–159.

Mempel, T. R., Pittet, M. J., Khazaie, K., Weninger, W., Weissleder, R., von Boehmer, H., von Andrian, U. H., 2006. Regulatory T cells reversibly suppress cytotoxic T cell function independent of effector differentiation. Immunity 25 (1), 129–41.

Miller, M. J., Safrina, O., Parker, I., Cahalan, M. D., 2004a. Imaging the single cell dynamics of $CD4^+$ T cell activation by dendritic cells in lymph nodes. J. Exp. Med. 200 (7), 847–856.

Miller, M. J., Wei, S. H., Cahalan, M. D., Parker, I., 2004b. T cell repertoire scanning is promoted by dynamics dendritic cell behavior and random T cell motility in the lymph node. Proc. Natl. Acad. Sci. USA 101 (4), 998–1003.

Mrass, P., Takano, H., Ng, L. G., Daxini, S., Lasaro, M. O., Iparraguirre, A., Cavanagh, L. L., von Andrian, U. H., Ertl, H. C., Haydon, P. G., Weninger, W., 2006. Random

migration precedes stable target cell interactions of tumor-infiltrating T cells. J. Exp. Med. 203 (12), 2749–61.

Scholer, A., Hugues, S., Boissonnas, A., Fetler, L., Amigorena, S., 2008. Intercellular adhesion molecule-1-dependent stable interactions between T cells and dendritic cells determine $CD8^+$ T cell memory. Immunity 28 (2), 258–70.

Schwickert, T. A., Lindquist, R. L., Shakhar, G., Livshits, G., Skokos, D., Kosco-Vilbois, M. H., Dustin, M. L., Nussenzweig, M. C., 2007. In vivo imaging of germinal centres reveals a dynamic open structure. Nature 446 (7131), 83–7.

Tadokoro, C. E., Shakhar, G., Shen, S., Ding, Y., Lino, A. C., Maraver, A., Lafaille, J. J., Dustin, M. L., 2006. Regulatory T cells inhibit stable contacts between $CD4^+$ T cells and dendritic cells in vivo. J Exp Med 203 (3), 505–11.